Time-resolved measurements of product formation in the low-temperature (550 – 675 K) oxidation of neopentane: a probe to investigate chain-branching mechanism

Arkke J. Eskola,[1,2] Ivan O. Antonov,[1] Leonid Sheps,[1] John D. Savee,[1] David L. Osborn,[1] Craig A. Taatjes[1,*]*

[1]*Combustion Research Facility, Sandia National Laboratories, 7011 East Avenue, MS 9055, Livermore, California 94551, USA*
[2]*University of Helsinki, Department of Chemistry, A.I. Virtasen Aukio 1, FI-00560 Helsinki, Finland*
[*]*corresponding authors: arkke.eskola@helsinki.fi, cataatj@sandia.gov*

Abstract: Product formation, in particular ketohydroperoxide formation and decomposition, were investigated in time-resolved, Cl-atom initiated neopentane oxidation experiments in the temperature range 550 K – 675 K using a photoionization time-of-flight mass spectrometer. Ionization light was provided either by the Advanced Light Source tunable synchrotron radiation or ~ 10.2 eV fixed energy radiation from a H_2-discharge lamp. Experiments were performed both at 1 – 2 atm pressure using a high-pressure reactor and also at ~ 9 Torr pressure employing a low-pressure reactor for comparison. Because of the highly symmetric structure of neopentane, ketohydroperoxide signal can be attributed to a 3-hydroperoxy-2,2-dimethylpropanal isomer, *i.e.* from a γ-ketohydroperoxide (γ-KHP). The photoionization spectra of the γ-KHP measured at low- and high pressures and varying oxygen concentrations agree well with each other, further supporting they originate from the single isomer. Measurements performed in this work also suggest that the "Korcek" mechanism may play an important role in the decomposition of 3-hydroperoxy-2,2-dimethylpropanal, especially at lower temperatures. However, at higher temperatures where γ-KHP decomposition to hydroxyl radical and oxy-radical dominates, oxidation of the oxy-radical yields a new important channel leading to acetone, carbon monoxide, and OH radical. Starting from the initial neopentyl + O_2 reaction, this channel releases altogether three OH radicals. A strongly temperature-dependent reaction product is observed at *m/z* = 100, likely attributable to 2,2-dimethylpropanedial.

Keywords: Neopentane, Autoignition, Ketohydroperoxide, Chain-Branching

1. Introduction

Autoignition of a premixed, very lean fuel-air mixture plays essential role in many advanced combustion strategies that promise to combine low emissions with high efficiency. The homogeneous charge compression ignition (HCCI) engine[1] is one prototypical example. Ignition timing in HCCI engine is controlled by autoignition of a charge upon compression and corresponding temperature rise. In other words, ignition timing is determined by chemical kinetics of a fuel-air mixture. Low-temperature oxidation chemistry, an essential part of a first state of ignition, plays an important role in determining ignition properties of a specific fuel-air mixture before the onset of a second state of ignition, where chain branching occurs by H_2O_2 decomposition, which leads to a rapid, final ignition.[2] The low-temperature oxidation chemistry that determines the time at which H_2O_2 decomposition temperature is reached is highly specific to the particular fuel molecule. This chemistry has a very significant effect on ignition timing in

HCCI engine: a major portion of total ignition time is determined by low-temperature oxidation. In the current work, low-temperature oxidation of neopentane (2,2-dimethyl propane) is investigated. Neopentane possesses significant low-temperature reactivity, described below, and has simple molecular structure, where all hydrogens are primary and identical. This simple molecular structure results in concise reaction product distribution under low-temperature combustion conditions where highly complex chemistry is often encountered. These properties make neopentane an ideal candidate to investigate low-temperature oxidation chemistry.

Low-temperature oxidation of a saturated hydrocarbon, e.g. neopentane, is initiated by formation of an alkyl radical R that further reacts with O_2. The R + O_2 reaction proceeds *via* formation of an alkylperoxy radical, RO_2, which can subsequently decompose back to reactants or isomerize:

$$R + O_2 \leftrightarrow RO_2 \rightarrow \text{products} \quad (1)$$

In addition, for an alkyl radical that has hydrogen(s) in β-position with respect to the radical site, both direct elimination from chemically excited RO_2 and thermal decomposition of RO_2 lead to formation of Q(alkene) + HO_2 products.

$$RO_2 \rightarrow Q + HO_2 \quad (2)$$

However, the radical of interest in this work, neopentyl radical $(CH_3)_3CCH_2$, does not have any β-hydrogen and thus reaction channel (2) forming an alkene is absent. This property makes neopentane an excellent radical source to investigate the chain-branching mechanism experimentally under low-temperature oxidation conditions where hydroperoxyalkyl radical QOOH plays a crucial role. Given the high symmetry of neopentane, relative simple potential energy surfaces (PESs) of R + O_2, QOOH + O_2, and HOOP=O (ketohydroperoxide, KHP) decomposition reactions can be drawn in a single plot, and a relatively small set of reactions can describe the initial steps of the low-temperature oxidation of neopentane, see Figure 1.[3]

Efficient formation of QOOH radical occurs when RO_2 isomerizes to QOOH *via* six-member transition state.[3, 4] This is also the lowest energy pathway from RO_2 and under low-temperature combustion conditions there is often an equilibrium between RO_2 and QOOH.

$$RO_2 \leftrightarrow QOOH \quad (3)$$

The carbon-centered QOOH radical (3-hydroperoxy-2,2-dimethylpropyl radical in case of neopentyl oxidation) can dissociate to QO (3,3-dimethyloxetane) and OH-radical in a chain-propagation reaction, see Figure. 1.

$$QOOH \rightarrow QO + OH \quad (4)$$

Other product formation channels are calculated to have barriers above the energy of the reactants and are not expected to play any significant role.[3, 4] However, in this work we observe isobutene formation even at low temperatures where unimolecular decomposition of neopentyl radical to isobutene and methyl radical is not important. In competition with reaction (4), QOOH radicals can react again with O_2, especially at high pressures ($p \geq 1$ atm) and high [O_2] conditions often encountered in practical combustion systems. Reaction (5) is essential for autoignition because it initiates a mechanism that leads to chain-branching, see figure 1.

$$QOOH + O_2 \leftrightarrow OOQOOH \quad (5)$$

The hydroperoxyalkylperoxy radical OOQOOH can efficiently isomerize to HOOPOOH radical which immediately decomposes to OH + HOOP=O, the latter of which is called ketohydroperoxide (KHP, here 3-hydroperoxy-2,2-dimethylpropanal) because it contains both ketone or aldehyde functionality and a hydroperoxy group.

$$OOQOOH \leftrightarrow HOOPOOH \rightarrow OH + HOOP=O \quad (6)$$

Ketohydroperoxide HOOP=O is a labile closed-shell molecule that can further thermally decompose and release the second OH radical (see Figure 1), effectively leading to chain-branching, *i.e.* together reactions (6) and (7) produce two OH radicals and an ȮPO radical.

$$HOOP=O \rightarrow OH + \dot{O}PO \quad (7)$$

Further reaction of the oxygen-centered ȮPO radical can also lead to reactive radicals and thus increase system reactivity even more. In this work investigations of further reactions of ȮPO play an important role.

Low-temperature oxidation of neopentane has received much attention before. Walker et al. added neopentane to slowly reacting mixtures of H_2/O_2 at 753 K and determined primary and secondary products under low-temperature oxidation conditions.[5-7] Their stated primary oxidation products were 3,3-dimethyloxetane, isobutene, acetone, and formaldehyde. They concluded that OOQOOH radical isomerization and decomposition is the source of acetone formation. Later they also performed temperature-dependent neopentane oxidation experiments using the same method.[8] Curran et al.[9] constructed a detailed chemical kinetic model on neopentane oxidation and simulated experimental results of Walker et al.[5-7]. Their model simulations were, in general, in good agreement with experimental results performed at 753 K. However, of interest to the current work, their model underpredicted methylpropanal formation and they suggested that there are probably other pathways leading to its formation. In a combined experimental and modelling flow reactor study of neopentane oxidation at 8 atmospheres, Wang and Curran et al.[10] both improved their model to fit experimental results performed over temperature range 620 – 810 K, but were unable to predict the significant formation of formic acid that was observed. Also interesting for the current work, significant [HCOOH] was observed already at the lowest experimental temperatures, 620 K, where no other reaction products were noticed, and the highest formic acid concentrations were measured around 650 K. Neopentane oxidation has also been studied in a temperature range 800 – 1230 K at 1, 5, and 10 atm pressures using the jet-stirred reactor (JSR) by Dagaut et al.[11], who also constructed a model to simulate their high-temperature experiments. Sun and Bozzelli[3] performed *ab initio* calculations at the CBS-Q level and carried out master equation analysis to evaluate reaction paths and kinetics for neopentyl oxidation. DeSain et al.[4] measured time-resolved production of OH and HO_2 radicals in the pulsed-photolytic Cl-atom initiated oxidation of neopentane in the temperature range 573 – 750 K and at total pressures about 55 Torr. They also simulated their low-pressure results using a small *ad hoc* kinetic model. Interestingly, they observed a significant (about 3 ×) increase in HO_2 production intensity at 673 K once $[O_2]$ was increased from 7 to 60×10^{16} cm^{-3}. Although their model was not able to describe the observation, they suggested that it originated from unspecified chain-branching reactions. Petway et al.[12]

extended measurements of DeSain et al. with some success, and modelled their results using the Reaction Mechanism Generator developed at MIT. Most recently Bugler et al.[13, 14] performed both rapid compression machine and shock tube experiments and revised the model thermochemistry and kinetics of pentane isomers' oxidation, resulting in very good agreement between modeled and experimental ignition delay times. Their neopentane oxidation model is used here to simulate current experiments performed at 1 – 2 atm pressures.

Although all neopentane oxidation models discussed above include a chain-branching mechanism where KHP formation and decomposition plays a crucial role, ketohydroperoxide has not been observed before in any neopentane oxidation experiments. KHP formation was observed for the first time fairly recently in low-temperature *n*-butane oxidation experiments[15] employing jet-stirred-reactor (JSR) and more recently ketohydroperoxide formation was observed in dimethyl ether oxidation measurements[16] using JSR. Time-resolved KHP formation and decomposition in low-temperature *n*-butane oxidation experiments were published only very recently.[17] KHP formation is observed in the current neopentane oxidation experiments; particular attention is focused on understanding the KHP decomposition mechanism, which might also proceed *via* mechanism(s) other than shown above in equation (7).

2. Experimental

In this study both low-pressure (p ~ 9 Torr) and high-pressure (p ~ 1 – 2 atm) flow reactors were employed. The low-pressure reactor has been described in detail before [18] and the high-pressure reactor (HPR) has been presented recently[17, 19]. Radical chemistry in the low- and high-pressure reactors was initiated by photolytic production of Cl-atoms which then reacted with neopentane producing neopentyl radicals in presence of O_2. In both the low- and high-pressure reactor 248 nm photolysis of oxalyl chloride ($(ClCO)_2 \xrightarrow{h\nu} 2\ Cl + 2\ CO$) was used to produce Cl-atoms while in a few high-pressure reactor measurements 193 nm photolysis of $CFCl_3$ ($CFCl_3 \xrightarrow{h\nu} CFCl_2 + Cl$) was employed due to high thermal and oxidative stability of $CFCl_3$. An uncoated tubular, heatable quartz reactor was used in low-pressure experiments. Most measurements with the HPR were performed using a more inert quartz tube in contact with photolytically initiated reacting mixture but a few experiments were carried out using a metal reactor. The low-pressure reactor is sampled *via* a ~ 650 µm hole on the tube wall (*i.e.* sampling is orthogonal to the photolysis laser beam and tubular reactor axis) whereas the HPR is sampled through a ~ 100 – 150 µm hole in the end-plate of the reactor (*i.e.* sampling is parallel with photolysis laser beam and tubular reactor axis). The sampled molecular beam from the reactors was then skimmed and intersected by ionizing vacuum ultraviolet (VUV) tunable radiation from the Advanced Light Source (ALS) synchrotron. Some experiments were also performed using ~10.2 eV radiation from a H_2-discharge lamp. Ionized species were mass-separated using an orthogonal-acceleration, multiplexed photoionization time-of-flight mass spectrometer (MPIMS) where full mass spectra were taken at 20 µs intervals to obtain time-resolved product spectra. Product spectra were typically collected up to 30 – 40 ms following photolytic initiation, over which time the experimental conditions (*e.g.* temperature) remained constant. In order to obtain quantitative information on branching ratios (BRs), time-resolved photoionization spectra were measured by scanning the energy of the ionizing synchrotron radiation.[20] BRs were then determined by fitting absolute photoionization cross-sections of pure compounds to time- and mass-integrated photoionization spectra and normalized to one product as a reference compound (here isobutene).[18]

The adiabatic ionization energy of 2,2-dimethylpropanedial was calculated at the CBS-QB3 level[21] with Gaussian 09 package[22]. To ensure that geometries were optimized at the global minima, the conformation space for both neutral and cation species was explored by scanning dihedral angles responsible for the orientation of two formyl rotors at ωB97XD/6-311G(2d,d,p) level[23]. All other internal degrees of freedom were allowed to optimize.

3. Results and Discussion

Scheme 1 shows a reaction mechanism developed by Wang et al. for neopentane low-temperature oxidation starting from neopentyl radical and extending up to the KHP formation.[10] Experiments in the current work were performed both at low and high pressure. While kinetics and yields of specific reactions in scheme 1 change with pressure and effect on observed product yields, the overall oxidation mechanism should not change, meaning that scheme 1 is in agreement with PESs of figure 1 and is applicable to interpret both low- and high-pressure results. Results of low-pressure experiments are discussed first since they help to interpret observations of high-pressure experiments. Table S1 shows products observed in the current experiments.

3.1 Low-pressure measurements. Figure 2 shows the time dependence of RO_2 and main products from Cl-atom initiated neopentane oxidation experiments performed at several temperatures using the low-pressure reactor. In these experiments, neopentylperoxy radical RO_2 was observed at the radical R = C_5H_{11} nominal mass at *m/z* = 71 (see fig. 2a), because the unstable RO_2^+ cation dissociates and produces R^+ in the ionization process. Except for a short period just after photolysis, the radical R concentration was always much smaller than [RO_2] and observed signal at *m/z* = 71 thus originated from RO_2. This is because at the high oxygen concentration employed the fast R + O_2 reaction resulted in rapid RO_2 formation. We estimate a lifetime of 0.02 – 0.06 ms for radical R after its rapid formation. At $T \geq 625$ K also equilibrium R + O_2 ↔ RO_2 as well as unimolecular decomposition R → CH_3 + isobutene starts to play a role.[4, 24] Because unimolecular decomposition of R is already fast at 625 K[24] and the concentration of O_2 is high, steady-state (ss) concentration of R remains low ($[R]_{ss}/[RO_2]_{ss} \approx 0.03$) and signal at *m/z* = 71 originates practically only from RO_2 (see also figure S1). Upon increasing temperature, the normalized signal intensity of RO_2 just after fast production decreases due to the combined effect of fast equilibrium R + O_2 ↔ RO_2 and increasingly rapid unimolecular decomposition R → CH_3 + isobutene. Also, RO_2 signal decay becomes faster due to increasingly fast and intense oxidation product formation as seen in figures 2b-c. At *m/z* = 56 product formation (see figure 2b) becomes faster and significantly more intense upon increasing temperature. At the photon energy employed, 10.6 eV, the signal at *m/z* = 56 originates both from the parent ion of isobutene and from the dissociative ionization of 3,3-dimethyloxetane. Isobutene and 3,3-dimethyloxetane are bimolecular products of two important chain-propagation channels in neopentane oxidation, see scheme 1. At higher temperatures, unimolecular decomposition of neopentyl radical also produces isobutene. The parent ion of 3,3-dimethyloxetane (*m/z* = 86) is highly unstable and decomposes almost entirely to $C_4H_8^+$ (*m/z* = 56) and CH_2O (*m/z* = 30) upon ionization. This can be seen from the absolute photoionization spectrum of 3,3-dimethyloxetane, which was determined in this work and is shown in figure S2.

Figure 3a shows the photoionization spectrum of *m/z* = 56 signal from an experiment at 625 K and 8.7 Torr pressure, integrated over 0 – 40 ms after laser initiation. The spectrum can be precisely fitted using absolute photoionization cross-sections of isobutene (parent ion) and 3,3-dimethyloxetane (daughter ion at mass 56) up to ~10.3 eV; dissociative ionization of the

neopentane precursor to form mass 56 hampers fitting to higher photon energies, see figure S3. Below photon energy ~ 9.45 eV only isobutene absorbs and figure S4 compares time-traces of isobutene (integrated over 8.9 – 9.45 eV) and isobutene + 3,3-dimethyloxetane (integrated over 8.9 – 10.35 eV). Within experimental uncertainty, the time-dependence of these signals agree precisely. This is an expected result since both isobutene and 3,3-dimethyloxetane are bimolecular products of parallel reaction channels, see Scheme 1.

Formaldehyde is the by-product of the chain-propagating channel with isobutene, see scheme 1. The time-dependence of the formaldehyde signal at different temperatures is shown in figure 2c. Especially at higher temperatures, the time-behavior of formaldehyde, the only compound at *m/z* = 30 as shown in figure 3b, agrees well with *m/z* = 56 behavior. Neither product shows a clear, fast initial rise followed by a slower formation (though *m/z* = 30 show some such behavior at 590 K). A fast initial rise would be associated with well skipping reaction on the PES, that is a reaction that proceeds from reactants to products without forming a thermalized RO_2, and the subsequent, slower formation would originate from decomposition of thermalized RO_2 to products.

Product formation at *m/z* = 118 in figure 2d is delayed formation with respect to products observed at *m/z* = 30 and *m/z* = 56. Considering that signals at *m/z* = 30 and *m/z* = 56 originate from primary products of Cl-atom initiated neopentane oxidation system, then product formation at *m/z* = 118 could be assigned as a secondary product. This time-behavior at *m/z* = 118 agrees with the suggestion that signal originates from a ketohydroperoxide, an important and most likely product of QOOH + O_2 reaction (see figure 1) and a key species in autoignition chemistry. The ketohydroperoxide at *m/z* = 118 is a γ-KHP, where one $–CH_2–$ group separates carbons containing an aldehyde and a hydroperoxy group. γ-KHP signals in figure 2d are relatively weak due to low oxygen concentration employed which is inherently limited by highest achievable pressures in low-pressure reactor (~ 10 Torr). Intensity of KHP signal increases with temperature up to 650 K after which signal intensity drops upon increasing temperature to 675 K. Figure S5a shows a signal that is observed at *m/z* = 100 at different temperatures. Probably the *m/z* = 100 signal originates from 2,2-dimethylpropanedial, which could be produced in a QOOH + O_2 → OOQOOH → HOOPOOH* → OH + HOOP=O* → OH + O=P_{-H} =O + H_2O water elimination reaction. Figure S5b shows a measured photoionization spectrum of the signal at *m/z* = 100 and 675 K. In the absence of absolute photoionization spectrum of 2,2-dimethylpropanedial, vertical ionization potential of $(CH_3)_2C(CHO)_2$, 9.8 eV,[25] measured using photoelectron spectroscopy, and the calculated adiabatic ionization energy of 9.39 eV can be compared with the spectrum of figure S5b. (The analogous molecule glyoxal shows a similar difference between vertical ionization potential and ionization energy.[26]) The agreement supports assignment of the *m/z* = 100 signal to $(CH_3)_2C(CHO)_2$.

In addition to the above products, an unexpected product was observed at *m/z* = 70, see figure 2e. At temperatures 590 – 650 K its formation is clearly fast, assigned above as formally direct product formation, with almost no slower formation from RO_2 thermal decomposition at longer reaction times. At 675 K slower formation is also clearly observed. Figure 2f shows the measured photoionization spectrum at *m/z* = 70 at 675 K, integrated over 0 – 40 ms after laser initiation. One possible product at nominal mass 70 would be methacrolein. However, its IE = 9.92 eV[26] does not agree with figure 2f, nor does IE = 9.65[26] eV of methyl vinyl ketone. Instead, adiabatic ionization energy measurements of 1,1-dimethyl cyclopropane, IE = 8.98 ± 0.05 eV (electron ionization measurement) and IE = 9.1 eV (photoelectron spectroscopy measurement) agree well with the spectrum of figure 2f. In addition, the lowest appearance energy determination of 1,1-dimethyl cyclopropane, forming $C_4H_7^+$ + CH_3 at energy 10.47 eV, is in agreement with the figure 2f

spectrum. Consequently, in the absence of absolute photoionization spectrum of 1,1-dimethyl cyclopropane, we suggest that observed product at *m/z* = 70 may originate from 1,1-dimethyl cyclopropane. This is an interesting observation and, if confirmed, would indicate that in the absence of a *β*-hydrogen, as in the current case of neopentane oxidation, formation of a cyclic alkane is a possible reaction channel. In the current case, reaction channel $(CH_3)_3CCH_2 + O_2 \rightarrow$ 1,1-dimethyl cyclopropane + HO_2 is exothermic about 12 kcal/mol, which can be compared with reaction channel $(CH_3)_3CCH_2 + O_2 \rightarrow RO_2$ that is exothermic about 38 kcal/mol. Value can also be compared with similar reaction channel involving a primary radical in *n*-butane oxidation, *n*-$C_4H_9 + O_2 \rightarrow$ 1-butene + HO_2, which is exothermic by about 18 kcal/mol.

Table 1 compares the branching ratios of oxidation products which were determined in this work experimentally at 575, 625, and 675 K temperatures relative to isobutene under constant total concentration conditions at low pressures. At 575 K formaldehyde (BR = 1.25) and isobutene (BR = 1 by definition) are the main products and BR of 3,3-dimethyloxetane is only about 0.45, although it is often considered as the main bimolecular product of neopentyl + O_2 reaction at low pressures.[4] BR of 2,2-dimethylpropanal is 0.16 and it could originate at least partly from radical – radical reactions; the transition state (TS) for its formation from R + O_2 is about 3 kcal/mol above the energy of the reactants, suggesting it is unlikely to be an important product of R + O_2 reaction. Other products have only small BRs at 575 K. At 625 K, formaldehyde BR remains about the same while BR of 3,3-dimethyloxetane increases significantly and is the same as that of formaldehyde within experimental uncertainty. This suggests that at 625 K and 8.7 Torr the reaction channels leading to 3,3-dimethyloxetane + OH and isobutene + CH_2O + OH are the main channels and are of equal importance. Increasing the temperature to 675 K has the effect of decreasing all BRs relative to isobutene, because RO_2 decomposes efficiently back to reactants and R subsequently partly decomposes to isobutene + CH_3 radical instead of reacting with O_2. Formaldehyde BR drops to 0.6 while BR of 3,3-dimethyloxetane decreases to a smaller degree, to 0.85. Again, BRs of other reaction products are small. Using the photoionization spectrum of figure 2f we can estimate a BR of the postulated product at *m/z* = 70, 1,1-dimethyl cyclopropane, by first assuming a value for its photoionization cross-section at certain energy (here at 10.5 eV), which is set to 9 Mb. This value can be compared with the following photoionization cross-sections at 10.5 eV: cyclopropane 9 Mb, propene 11.5 Mb, and isobutene 11 Mb. Using formaldehyde as reference, a BR ~ 0.08 for 1,1-dimethyl cyclopropane relative to isobutene is obtained at 675 K, 9.4 Torr. Although this value is highly uncertain, comparing this value with Table 1 BRs indicates that 1,1-dimethyl cyclopropane is not a major reaction product.

3.2 High-pressure measurements. Measurements at high pressures (*i.e.* $p \geq 1$ atm) are essential to understand autoignition chemistry of combustion systems from several reasons. Practical combustion apparatuses, e.g. HCCI-engines, operate at high pressures. Kinetic models of autoignition and combustion chemistry are almost always developed and optimized for high pressure engine conditions and their applicability to simulate low-pressure experiments is often limited. Experiments performed at low pressures (p ~ 10 Torr) are also inherently limited by highest achievable oxygen concentration; at 600 K and 10 Torr $[O_2]_{max} \sim 1 \times 10^{17}$ cm^{-3} can be compared with $[O_2]_{max}$ at 600 K and 1 atm ~ 1×10^{19} cm^{-3} and 2 atm ~ 2×10^{19} cm^{-3}. Oxygen concentration is important parameter because of its role in interception of QOOH radicals in reaction (5) that leads to KHP formation. Understanding KHP formation and decomposition kinetics and mechanism are essential for reliable autoignition modelling.

In these experiments, the highest feasible temperature for a certain reaction system using the HPR is limited by auto-oxidation of a reactant mixture, i.e. ongoing oxidation without a photolytic initiation. In the current neopentane oxidation experiments at $p \geq 1$ atm, spontaneous oxidation was observed at $T \geq 700$ K, *i.e.* significant neopentane oxidation and product formation occurred without laser initiation. In these experiments, stable $CFCl_3$ photolytic precursor was used.

Figure 4 shows results from Cl-atom initiated neopentane oxidation experiments which were performed using the HPR at 1 atm pressure and employing single photon energies of 9.8, 10.2, and 11.7 eV. It can be seen from figure 4a that time-dependent signal at *m/z* = 56, which originates from isobutene and 3,3-dimethyloxetane as discussed before, shows some intensity already at 550 K and the intensity increases upon increasing temperature to 600 K until at 650 K signal also exhibits an increase with time after first ~ 10 ms following laser initiation. Figure 4b shows the temporal behavior of the signal at *m/z* = 118, originating from KHP, at different temperatures. In comparison to figure 2d, KHP is formed significantly faster under 1 atm and ~ 60 times higher $[O_2]$ conditions. Under high pressure conditions KHP formation (at *m/z* = 118) and product formation at *m/z* = 56 have similar time-behavior. This similarity of timescales has also been observed in *n*-butane oxidation experiments.[17] As expected, KHP signal intensity with respect to other products also increases significantly at higher pressure. In the current case, $[KHP]/[RO_2]$ ratio, measured as $I(m/z = 118)_{t = 30\ ms} / I(m/z = 71)_{t = 1\ ms}$, becomes about 27 times larger upon increasing pressure from 10 Torr to 1 atm and $[O_2]$ from 5×10^{16} cm^{-3} to 2.85×10^{19} cm^{-3}, as measured by comparing signal intensities of figures 2b and 4b. Figure 5 compares KHP formation kinetics and photoionization spectra at different pressures and temperatures. It can be seen from figure 5a that simultaneous increase in total pressure (× 100) and $[O_2]$ (× 50) at 625 K has a relatively small effect on the time profile of KHP formation (but more significant effect on intensity). The change in timescale was more pronounced in case of *n*-butane oxidation.[17] While KHP formation at low pressure is slower and has significantly lower intensity than at high pressure, the photoionization spectra of KHP collected at varying conditions agree precisely within experimental uncertainty, further supporting the assignment of signal at *m/z* = 118 as KHP for all conditions.

Figures 4c and 4d display the formation of products that potentially originate from KHP decomposition. Scheme 2 shows two mechanisms for the decomposition of γ-KHP (3-hydroperoxy-2,2-dimethylpropanal). Decomposition of γ-KHP *via* -O–OH bond rupture to two radicals, OH + ȮPO (reaction 7), to the left from γ-KHP in Scheme 2, is the well-known KHP decomposition mechanism leading to chain-branching and is included in any kinetic model of fuel low-temperature oxidation. On the other hand, γ-KHP decomposition *via* isomerization to a cyclic peroxide intermediate and subsequent decomposition of the cyclic peroxide to a carbonyl compound and an organic acid (to the right from γ-KHP in Scheme 2), known as a Korcek decomposition, has been suggested[27] only very recently. The importance of this mechanism in gas phase chemistry is still uncertain and experimental work is needed to quantify its contribution. The Korcek decomposition makes the overall reaction chain starting from neopentyl + O_2 a chain-propagation reaction mechanism, because it simply converts one closed-shell species to two closed shell species (note that one hydroxyl radical is formed in reaction (7)). This is very different from the KHP decomposition *via* -O–OH bond rupture, which is a chain-branching reaction mechanism and accelerates system reactivity. Figures 4c and 4d show product formation at masses 46 and 72, which were measured at 11.7 and 9.8 eV photon energies at three temperatures. Both signals have the time-behavior of a tertiary product, *i.e.* signal time-derivative at $t = 0$ is zero, and signals have similar time-profiles. At 650 K the temporal profiles overlap, see figure 6b, and as shown in figures

6c and 6d, *m/z* = 46 signal originates from formic acid and *m/z* = 72 signal almost entirely from methylpropanal. According to Scheme 2, these are the Korcek decomposition products of 3-hydroperoxy-2,2-dimethylpropanal. Figure S6 shows *m/z* = 46 and 72 signals of figures 4c and 4d, which clearly overlap precisely at each temperature and their formation becomes faster with increasing temperature, supporting their origin in the suggested reaction. There is also a very weak product signal at *m/z* = 88 at 650 K. However, this signal is far too weak to be fitted and consequently cannot be assigned to isobutyric acid, for example, and due to several sources of formaldehyde observed, no product can be assigned solely to formaldehyde and isobutyric acid channel of Scheme 2.

Figures 4e and 4f display formation of products at masses 58 and 70, which are attributed to KHP decomposition and subsequent reactions, see Scheme 3. Signal at *m/z* = 58 in figure 4e originates solely from acetone; other potential isomers have higher ionization energies than the 9.8 eV photon energy that is employed (*IE*(CH_3COCH_3) = 9.7 eV, *IE*(CH_3CH_2CHO) = 9.96 eV, and *IE*(Methyloxirane) = 10.2 eV).[26] It is clear from figure 4e that acetone formation is very small at 550 and 600 K until at 650 K a dramatic increase in signal intensity is observed. By comparing time-behavior of KHP signal (*m/z* = 118, figure 6a) and Korcek decomposition products signals (*m/z* = 46 and 72, figure 6b) with temporal behavior of acetone signal (*m/z* = 58, figure 6a), it can be observed that at 650 K acetone signal formation is even more delayed than that of the Korcek decomposition products. This is in accordance with the mechanism in Scheme 3, where acetone formation requires more kinetic steps, including one additional reaction with O_2, than formation of products at *m/z* = 46 and 72. Similarly to low-pressure experiments, rapid product formation at *m/z* = 70 is also observed in the HPR experiments, see figure 4f, where a clear yet weak signal appears already at the lowest experimental temperature, 550 K. There is very little change in its intensity or time profile upon heating to 600 K. However, heating from 600 K to 650 K has a strong effect, similar to that observed for acetone. At 650 K signal at *m/z* = 70 increases linearly after fast formation within ~ 2 ms after photolysis. This slow formation is consistent with methacrolein forms according to Scheme 3. Figure S7 shows the temporal trace of formaldehyde at different temperatures from the same set of experiments as the traces in figure 4. As shown in Scheme 3, formaldehyde is an intermediate product of the reaction mechanism leading to formation of both acetone and methacrolein.

Table 2 shows experimental BRs, relative to isobutene, from measurements performed at 650 K and 1060 Torr pressure using 248 nm photolysis of $(ClCO)_2$ as Cl-atom source. Similar to BRs in the low-pressure measurements, formaldehyde, 3,3-dimethyloxetane, and isobutene are the main products. However, formaldehyde BR, 3.0 ± 0.34, is now much higher than the approximate unity BR at low pressures, while BR of 3,3-dimethyloxetane, 1.64 ± 0.33, is slightly higher than its unity BR at low pressures. Comparison of BRs of low- and high-pressure measurements shows the emergence of new important reaction products, namely acetone, formic acid, and methyl propanal in the HPR measurements. These products and their temperature dependences were already discussed above and now their BRs at one temperature, 650 K, have also been determined. The branching to acetone is significant and the fairly unreactive acetone product is also a marker of the reaction channel which leads to formation of three OH radicals for one neopentyl radical. Significant yields of formic acid and methyl propanal support the current suggestion that Korcek decomposition of γ-KHP plays an important role in autoignition chemistry of neopentane.

3.3 Simulations of the HPR conditions and comparison with the current data. Time- and species-resolved information of product formation in photolytically initiated oxidation of a fuel

under low-temperature combustion conditions provides an excellent test-bench for kinetic models of combustion. Bugler et al. have very recently revised the kinetics and thermodynamics of the low-temperature oxidation of alkanes[13] and ignition delay times of *n*-pentane, *iso*-pentane, and *neo*-pentane mixtures were used as validation target for their kinetic model[14]. Their up-to-date model is used here in kinetics simulations to interpret current HPR experiments and conditions as well as enabling comparisons with the model.

Current interest in HPR experiments and simulations is centered on formation and decomposition of γ-KHP as well as on formation of subsequent products. First simulations revealed that without any modification to the gas-phase kinetic model of Bugler et al., the simulated KHP signal starts to deviate increasingly from the experimental signal around 10 ms after photolytic initiation, see figure S8. The simulation predicts that KHP continues to increase linearly also after ~10 ms, whereas the experimental time trace reaches a maximum at about 30 ms after photolysis and decreases afterwards. The disagreement between the simulated and experimental KHP signal implies that an additional sink-term of γ-KHP that does not form OH must be added to the model. At around 1 atm pressure a first-order removal rate coefficient of 58 s^{-1} was found to deliver near-perfect agreement between experimental and simulated γ-KHP signals. As seen from figure S8, experimental and simulated time-behavior of other main products also agree well within experimental uncertainty. This additional sink term with rate coefficient of ~ 58 s^{-1} at about 1 atm pressure and in the temperature range ~ 575 – 650 K matches the prediction for a diffusion-limited loss of the KHP on reactor walls, *i.e.* assuming all KHP molecules that reach the reactor wall react rapidly and do not produce OH. Peroxides are known to easily decompose on heated surfaces already below 500 K, supporting current use of a diffusion-limited loss of the γ-KHP on reactor walls in simulations over entire temperature range of this work, 550 – 675 K.[28] At 2 atm pressures diffusion-limited loss of the KHP on reactor walls with a rate ~ 29 s^{-1} was employed because diffusion coefficient is inversely dependent on pressure.

In figure 4b experimental γ-KHP signals at three temperatures have been simulated and good agreement is obtained at each temperature. Note that model can simulate changes in KHP signal intensity as temperature is changed. At 650 K more intense signal at longer times is simulated than is observed experimentally. Important for the current work, a very strong temperature dependence of acetone formation is also predicted by the model. BRs at 650 K, 1060 Torr pressure discussed above were also simulated using Bugler et al. model and diffusion-limited loss of the KHP on reactor walls, 58 s^{-1}, see table 2. In general, there is good agreement between experimental and simulated BRs for the main oxidation products. The experimental BR of formaldehyde, $BR(CH_2O)_{exp.} = 3.0 \pm 0.34$, agrees with the simulated value 2.77 within stated uncertainty and both values are much higher than at low pressures. Note that uncertainties shown refer only to a fitting uncertainty. The difference between the measured $BR(3,3\text{-dimethyloxetane})_{exp.} = 1.64 \pm 0.33$ and the simulated value of 2.50 is larger than stated uncertainty. The difference between $BR(\text{acetone})_{exp.} = 0.75 \pm 0.10$ *versus* 1.06 from simulations can be considered as being in good agreement, especially since acetone is formed "late" in neopentane oxidation process. Larger discrepancies appear for other products. Because $BR(\text{methacrolein})_{exp.} < 0.04 \pm 0.01$ is actually an upper limit due to presence of some 1,1-dimethyl cyclopropane in *m/z* = 70 signal as figure 4f suggest, simulations predict over three times more methacrolein than is observed in the experiments. Observed $BR(HCOOH)_{exp.} = 0.40 \pm 0.07$ is about twice the simulated value. This might suggest that other half originates from Korcek decomposition discussed above, because Bugler et al. model does not include Korcek decomposition mechanism. Methylpropanal is the accompanying product of the Korcek decomposition of γ-KHP, see Scheme 2, for which $BR_{exp.} =$

0.90 ± 0.18 is much higher than potential BR(HCOOH) ≈ 0.2 from Korcek decomposition. The kinetic model of Bugler et al. predicts essentially no methylpropanal formation. This suggests that relatively large, slow formation path of methylpropanal is missing. A surface reaction, for example γ-KHP decomposition on reactor walls, could conceivably be responsible for this slow formation, see simulated trace in figure S8. Also $BR(propene)_{exp.} = 0.39 \pm 0.07$ is significant, yet simulations predict essentially no propene formation. The time-profile of propene formation, however, is similar to γ-KHP formation and therefore must have source(s) other than surface reactions.

Discrepancies between experimental and simulated BRs of the main products (formaldehyde, 3,3-dimethyloxetane, and acetone) necessitate further discussion. All BRs were determined with respect to isobutene and any difference in yield of isobutene between experiments and simulations would then influence all the above BRs. In low-pressure experiments significant isobutene formation is observed already at 575 K and 8 Torr where the measured $BR(3,3\text{-dimethyloxetane})_{exp.} = 0.45 \pm 0.05$ with respect to isobutene, see Table 1. Increasing temperature to 625 K increases $BR(3,3\text{-dimethyloxetane})_{exp.}$ to 1.21 ± 0.06. In light of the PES of R + O_2 reaction shown in figure 1, this is an unexpected result because TS leading to 3,3-dimethyloxetane + OH products is about 4.5 kcal/mol below the energy of the reactants while TS leading to isobutene + H_2CO + OH products is about 5.4 kcal/mol above the energy of the reactants. According to PES of figure 1, one would expect much larger than unity BR(3,3-dimethyloxetane) with negative temperature dependency but reverse is observed experimentally. Neopentane oxidation experiments of Wang and Curran et al.[10] indicate that BR of 3,3-dimethyloxetane with respect to isobutene is below unity at 650 K, 8 atm and has a positive temperature dependency, broadly supporting current results. Small discrepancies between experimental and simulated BRs of the main products in the current work could be significantly reduced, if not removed, by reducing yield of 3,3-dimethyloxetane + OH channel in simulations about 20 % and increasing yield of isobutene + H_2CO + OH channel correspondingly about 20 %.

The simulated BR(γ-KHP) = 2.36 is substantial (remember that γ-KHP sink-term, 58 s^{-1}, was included in these simulations) and photoionization spectrum at *m/z* = 118, see figure 5, almost certainly originates from the γ-KHP. However, because of the lack of absolute photoionization spectrum of γ-KHP formed in neopentane oxidation, or more generally, lack of absolute photoionization spectrum of *any* KHP, measured spectrum at *m/z* = 118 cannot be converted to concentration or branching ratio. Very recently Rodriguez et al.[29] estimated absolute photoionization cross-sections of several hydroperoxides, including ketohydroperoxide $C_5H_{10}O_3$ that they observed at ~ 600 K in atmospheric-pressure JSR measurements of *n*-pentane low-temperature oxidation. Their estimated photoionization cross-section of $C_5H_{10}O_3$ ketohydroperoxide, 14.59 Mb at 10.6 eV and 20.55 at 11.0 eV, is the same for *n*-pentane and neopentane oxidation KHP isomers, 4-hydroperoxy-2-pentanone and 3-hydroperoxy-2,2-dimethylpropanal, respectively. Their method for estimating cross-sections would indicate a significant change in KHP ionization cross-section upon increasing photon energy from 10.6 eV to 11.0 eV, which is not supported by the current measurements, see figure 5b. Using absolute photoionization cross-section of $C_5H_{10}O_3$, 14.59 Mb at 10.6 eV, would imply $BR(\gamma\text{-KHP})_{exp} \approx 0.14$ at 650 K and 1060 conditions, see table 2. This BR is much lower than simulated BR(γ-KHP) = 2.36 and suggests either that absolute photoionization cross-section of γ-KHP formed in neopentane oxidation experiments is substantially smaller than above estimate, or that the model dramatically overestimates γ-KHP formation. Moreover, as in the absolute photoionization cross-section measurements of 3,3-dimethyloxetane (figure S2) and neopentane (figure S3), it is possible that 3-hydroperoxy-2,2-dimethylpropanal dissociates during ionization and parent ion intensity is

consequently small. Measurement of the absolute photoionization cross-section of γ-KHP would certainly be invaluable for determining $BR(\gamma\text{-KHP})_{exp}$.

To test the kinetic model at still higher temperatures, a further set of experiments was carried out under constant total-density conditions using a more inert $CFCl_3$ photolytic precursor, enabling measurements up to 675 K temperature at 1 atm pressure, see figure 7. Experimental time-traces at masses 58 and 118 were simulated as before, *i.e.* using KHP sink-term with rate 58 s^{-1}. There are significant changes in intensities of *m/z* = 56, 58, and 100 signals upon increasing temperature from 650 K to 675 K, only 25 K. On the other hand, γ-KHP signal at *m/z* = 118 shows little change when temperature is increased from 650 K to 675 K; KHP formation is slightly faster at higher temperature. Simulated time-traces of KHP are in good agreement with experiments up to 650 K while at 675 K KHP is predicted to decompose more rapidly than experiments indicate. Experimental signal at *m/z* = 58, originating from acetone according to Scheme 3, shows very strong increase in intensity once temperature is increased from 650 K to 675 K. The kinetic model of Bugler et al.[13, 14] is able to predict both the time-behavior and increase in intensity of *m/z* = 58 signal when temperature is changed.

Similar to the observation in the low pressure reactor measurements above, product formation at *m/z* = 100 is also observed in the HPR measurements, see figure 7c. As suggested above, HPR measurements are also consistent with the *m/z* = 100 signal originating from 2,2-dimethylpropanedial, which could be produced in $QOOH + O_2 \rightarrow OOQOOH \rightarrow HOOPOOH^* \rightarrow OH + HOOP{=}O^* \rightarrow OH + O{=}P_{\text{-H}}{=}O + H_2O$ water elimination reaction. The signal at *m/z* = 100 possesses very strong dependence on temperature and the temporal behavior of the signal close to *t* = 0 is different from that at *m/z* = 58; the time derivative of *m/z* = 100 signal at *t* = 0 is non-zero at 675 K. If the 2,2-dimethylpropanedial arises from a rapid decomposition of chemically activated KHP, as above, it may follow the time behavior of KHP near *t* = 0. Because 2,2-dimethylpropanedial likely does not decompose on reactor walls similar to KHP, the time-behavior of signal at *m/z* = 100 could be similar to that of KHP without decomposition on walls, see figure S8 and a simulation using unmodified model. Simulated time-behavior is linear with non-zero time-derivative at *t* = 0, in agreement with signal in figure 7c. In the model of Bugler et al. no products with *m/z* = 100 are included.

The suggestion that dials (and more generally diones) could be formed in a parallel (but higher activation energy) reaction channel from KHP is a new idea, although dials are very often observed in low-temperature combustion experiments. For example Rodriguez et al.[29], Pelucchi et al.[30], and Bugler et al.[31] test and use different reactive routes to predict formation of dials/diones with some success but have difficulty explaining their preferential formation at higher temperatures than ketohydroperoxides. The suggested mechanism may solve this problem.

Finally a set of experiments was performed to investigate the effect of changing $[O_2]$ on KHP formation, see figure 8. Experiments were performed at about 2 atm total pressure and 575 K temperature. Because of the higher total pressure, 2 atm, diffusion-limited loss of the KHP on reactor walls with rate ~ 29 s^{-1} was employed. Increasing $[O_2]$ under constant temperature and pressure conditions significantly increases KHP signal intensity whereas signal time-profile does not change to any significant extent. Signal time-behavior was also modelled using Bugler et al. model. It can be seen from figure 7 that model reproduces signal time-behavior well yet it slightly overestimate intensity dependence on $[O_2]$. Under the conditions of figure 8, KHP signal intensity increases with factor 1.6 as $[O_2]$ is doubled, as shown in figure S9. Due to complexity of the system, it is likely this is a result of several competing reactions.

As was already noted in the introduction section, in their detailed modelling work of the experiments from Walker et al.,[5, 6] Curran et al.[9] observed more methyl propanal formation than their model was able to predict; we can now suggest that at least some portion of methyl propanal originated from the Korcek decomposition of γ-KHP. The Korcek decomposition was not included in the Curran et al.[9] model. Similarly, in a combined experimental and modelling flow reactor study of neopentane oxidation, Wang and Curran et al.[10] observed a significant formation of formic acid, which their model was not able to predict. Note that their model did not include Korcek decomposition mechanism nor was methyl propanal measured in their experimental setup. The current and Wang and Curran et al.[10] observations are in agreement with the Korcek decomposition of γ-KHP to form formic acid and methyl propanal through a reaction channel with lowest rate-limiting energy barrier, which is effective already at temperatures where γ-KHP decomposition via -O–OH bond rupture is negligible. This low-barrier (but relatively low entropy) Korcek channel is in agreement with theoretical results of Jalan et al.[27]. The model of Bugler et al.[13, 14] employed in the current work did not include the Korcek decomposition mechanism.

For better comparisons between results of neopentane oxidation experiments and model simulations, absolute photoionization cross-sections of several products (γ-KHP, dimethyl propanedial, 1,1-dimethyl cyclopropane, etc.) would be needed.

4. Conclusions

In this work KHP formation under neopentane low-temperature oxidation conditions was observed experimentally for the first time. In addition, potential products of Korcek decomposition of γ-KHP were observed, suggesting that recent theoretically predicted mechanism play a role in gas-phase neopentane oxidation. Although the major neopentane Korcek decomposition products, formic acid and methyl propanal, have been observed previously, in this work these products are observed simultaneously in time-resolved manner, providing new experimental support for this mechanism. At higher temperatures γ-KHP decomposition via -O–OH bond rupture dominates and subsequent reactions of oxy-radical formed results in formation of acetone, carbon monoxide, and OH radical. Time-resolved signals of γ-KHP and acetone were measured at several temperatures up to a temperature close to conditions of spontaneous oxidation. Both time behaviors and intensities of γ-KHP and acetone signals were simulated using NUIGMech_C5_July2015 model and good agreement was observed between results of experiments and model simulations. Strong positive temperature dependency was noticed for formation of ternary product acetone. Formation of a product was observed at m/z = 100, potentially originating from 2,2-dimethylpropanedial, which positive temperature dependency was even stronger than for acetone. Time behavior of γ-KHP and product at m/z = 100 were similar and secondary to RO_2 signal at early times, suggesting 2,2-dimethylpropanedial is formed in a chemically activated QOOH + O_2 reaction in parallel with of γ-KHP.

5. Acknowledgements

This material is based upon work supported by the U.S. Department of Energy, Office of Science, Office of Basic Energy Sciences (DOE/BES). Part of work of A.J.E. is supported by the Academy of Finland, Grant No. 288377. I.O.A and L.S. are supported by DOE/BES under the Argonne-Sandia Consortium on High-Pressure Combustion Chemistry. Sandia is a multiprogram laboratory operated by Sandia Corporation, a Lockheed Martin Company, for the United States Department of Energy's National Nuclear Security Administration under contract DEAC04-94AL85000. This work used resources of Advanced Light Source, an Office of Science User Facility supported by

the Director, Office of Science, Office of Basic Energy Sciences, of the U.S. Department of Energy under Contract No. DE-AC02-05CH11231.

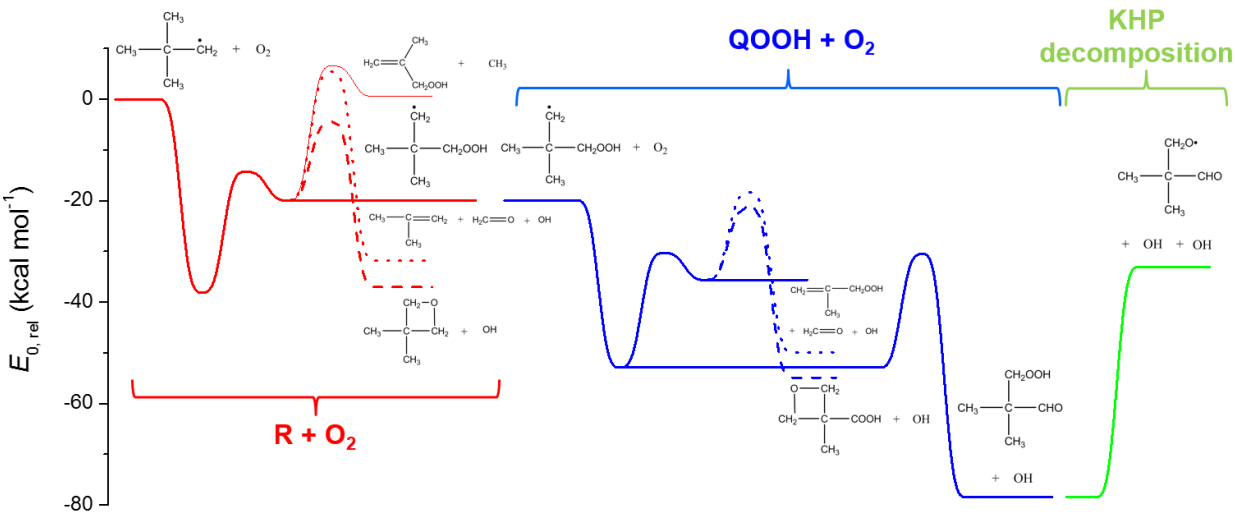

Figure 1. Potential energy surfaces of R + O_2, QOOH + O_2, and ketohydroperoxide (KHP) decomposition reactions according to a current understanding of neopentane chain-branching mechanism under low-temperature combustion conditions (R = neopentyl radical). Energies are taken from Sun and Bozzelli.[3]

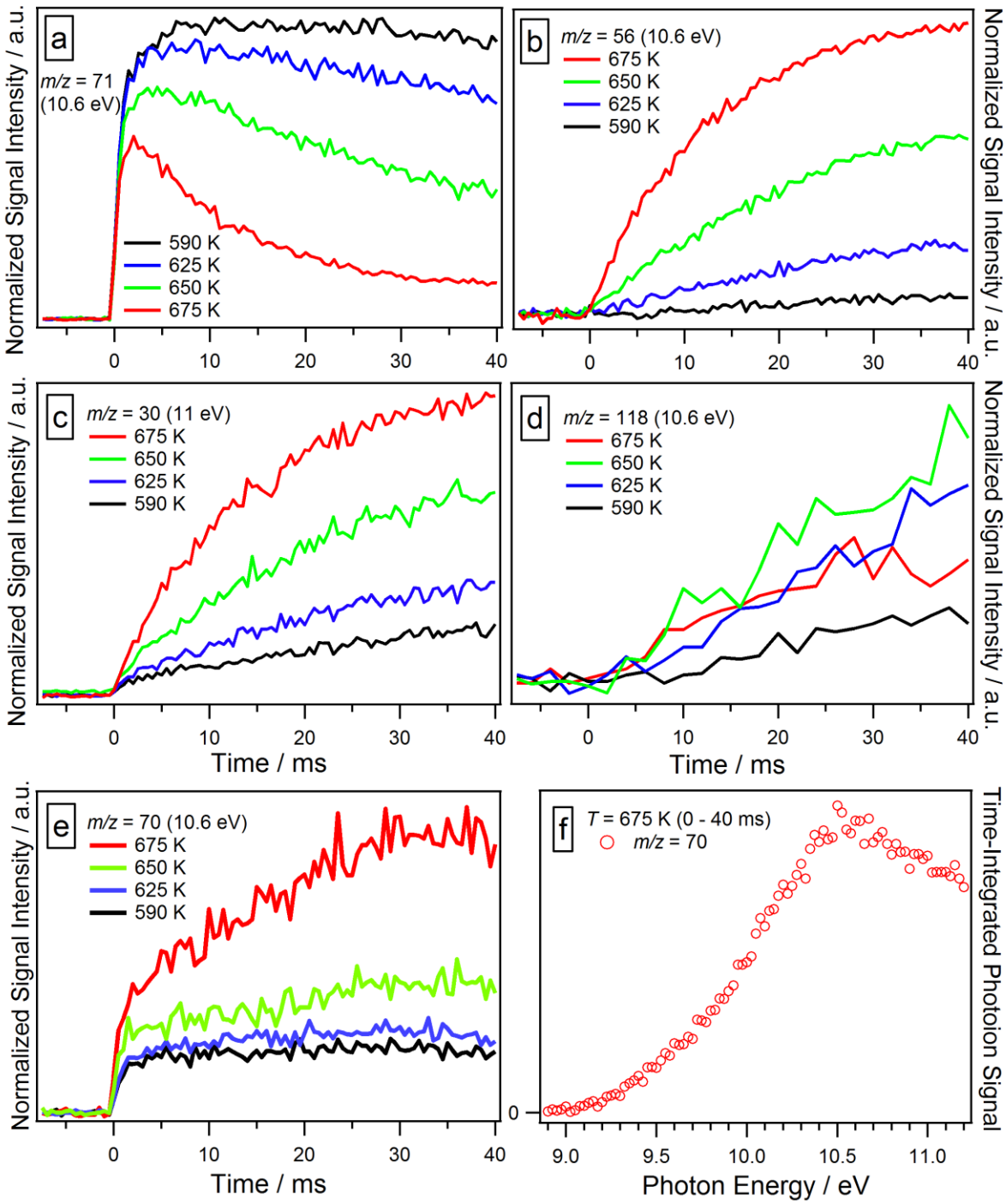

Figure 2. Time traces of main products from Cl-atom initiated neopentane oxidation experiments performed at different temperatures using the low-pressure reactor ([O_2] = 5 × 10^{16} cm^{-3}, *P* = 10 Torr). **a**) Neopentylperoxy radical RO_2 observed at *m/z* = 71. **b**) Signal at *m/z* = 56 originates from *i*-butene and 3,3-dimethyloxetane. **c**) Signal at *m/z* = 30 originates from formaldehyde. **d**) Signal at *m/z* = 118 comes from *γ*-KHP. **e,f**) Time-dependence of signal observed at *m/z* = 70 and its time-integrated signal *versus* photon energy at 675 K. Normalization is done using neopentane signal at *m/z* = 56 before firing laser.

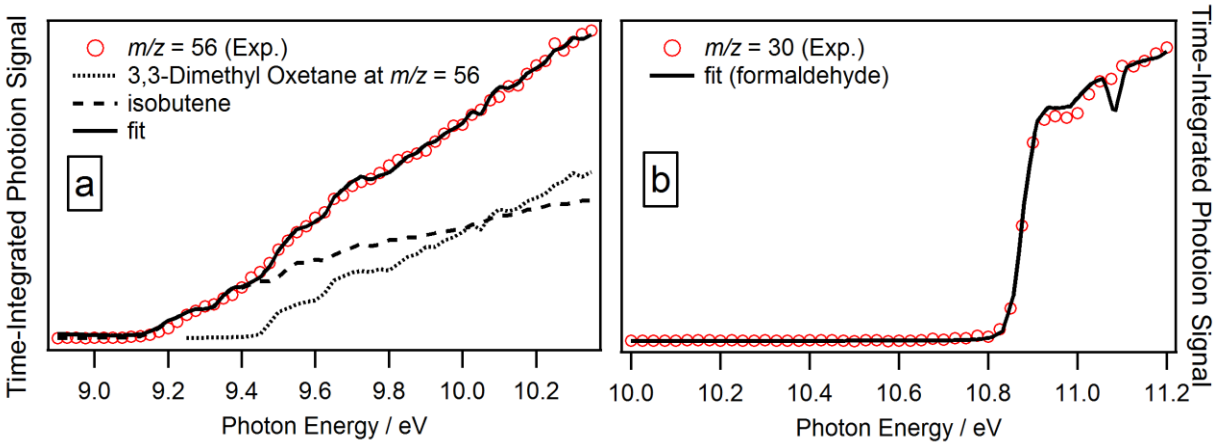

Figure 3. Photoionization spectra of the important products at *m/z* = 56 and *m/z* = 30 from Cl-initiated neopentane oxidation at 625 K, 8.7 Torr, and $[O_2] = 5 \times 10^{16}$ cm^{-3}. **a**) Situation is complex at *m/z* = 56 where, in addition to isobutene signal, a strong contribution from a daughter ion of 3,3-dimethyloxetane (molecular mass = 86u) is observed; this compound does not, effectively, have any signal at the parent mass, see figure S2. Daughter ion signal at *m/z* = 56 is used to determine 3,3-dimethyloxetane branching ratio. **b**) Fitting of a signal at *m/z* = 30 using a formaldehyde spectrum only.

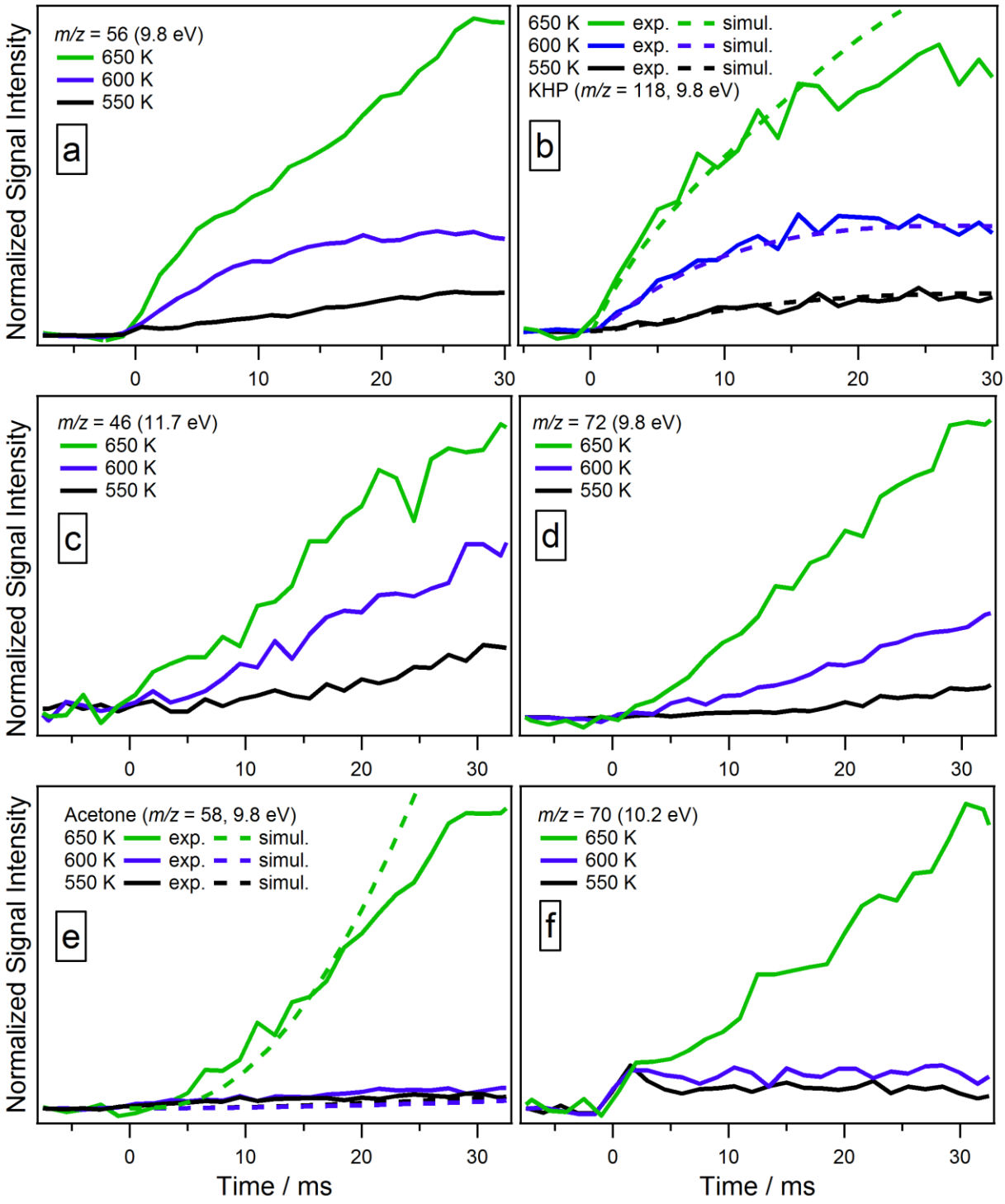

Figure 4. Comparison of time traces from a same set of Cl-atom initiated neopentane oxidation experiments performed under constant density conditions ($[O_2] = 2.85 \times 10^{18}$ cm^{-3}) at about 1 atm pressure to investigate kinetics and mechanism of γ-KHP formation and subsequent reactions under conditions close to autoignition temperature. KHP and acetone formation in (**b**) and (**e**) are simulated using NUIGMech_C5_July2015 model for comparison, see text for details.

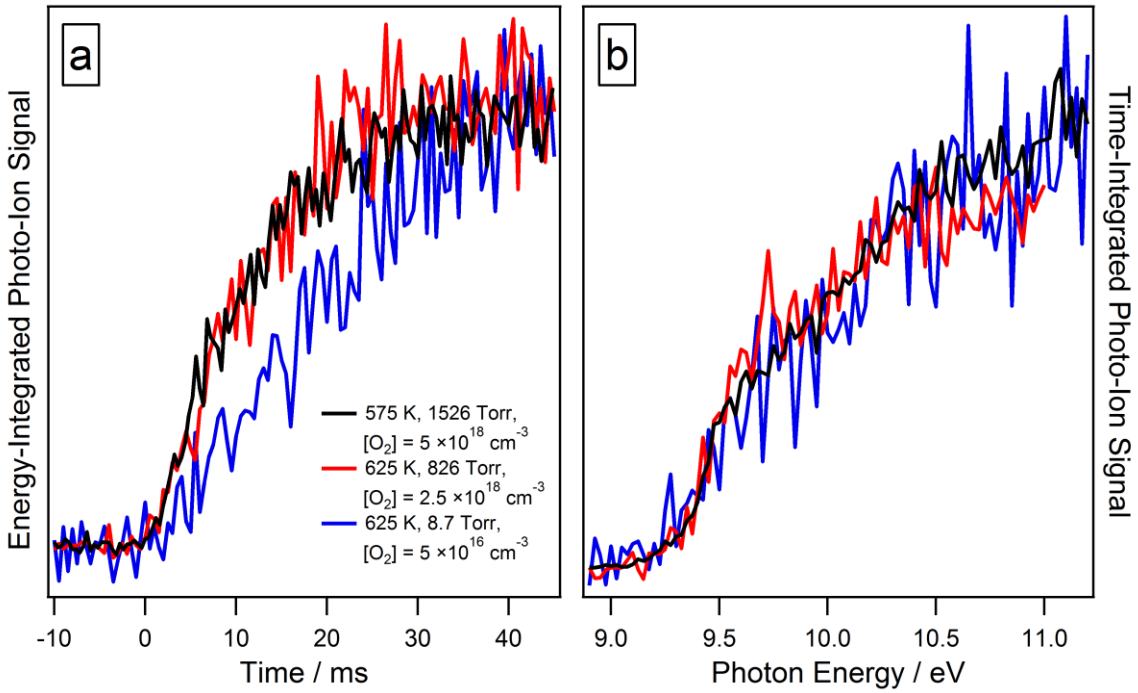

Figure 5. Formation kinetics (**a**) and photoionization spectra (**b**) of the γ-KHP observed at *m/z* = 118 in the low- and high-pressure Cl-initiated neopentane oxidation experiments performed in the current work.

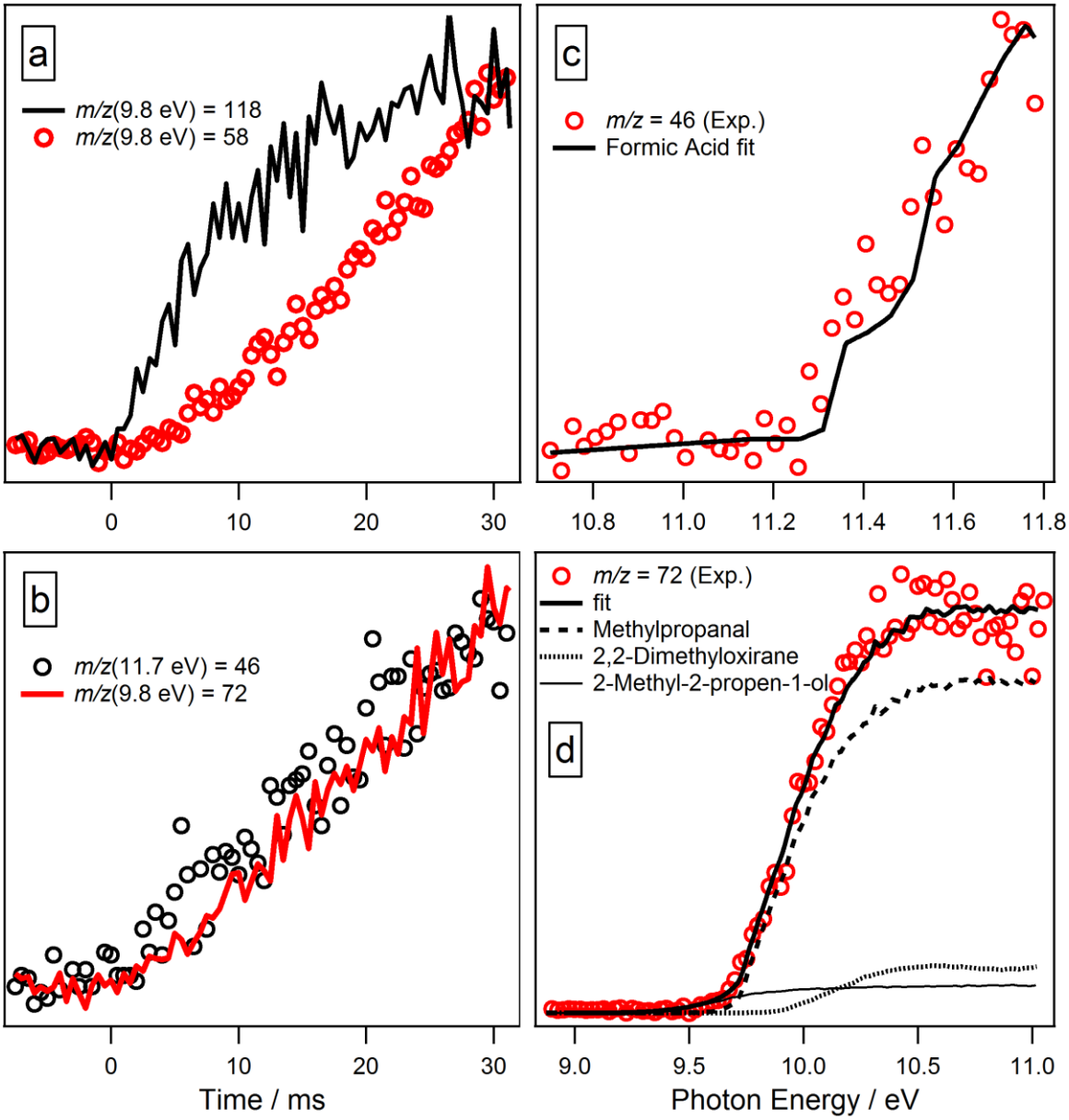

Figure 6. Selected time traces to construe decomposition mechanisms of γ-KHP at 650 K and 1060 Torr pressure ($[O_2]$ = 2.85 × 10^{18} cm^{-3}) in neopentane oxidation. **a**) Comparison of γ-KHP to acetone (*m/z* = 58, 9.8 eV) signal. **b**) Time-behavior of formic acid (*m/z* = 46) and methyl propanal (*m/z* = 72) agree and show different behavior from that of γ-KHP and acetone. Note that acetone formation is delayed with respect to formic acid and methyl propanal formation, suggesting they are earlier products than acetone. **c,d**) PIE spectra of *m/z* = 46 (11.7 eV) and 72 (9.8 eV) signals originate from formic acid and methyl propanal (>90 %), respectively.

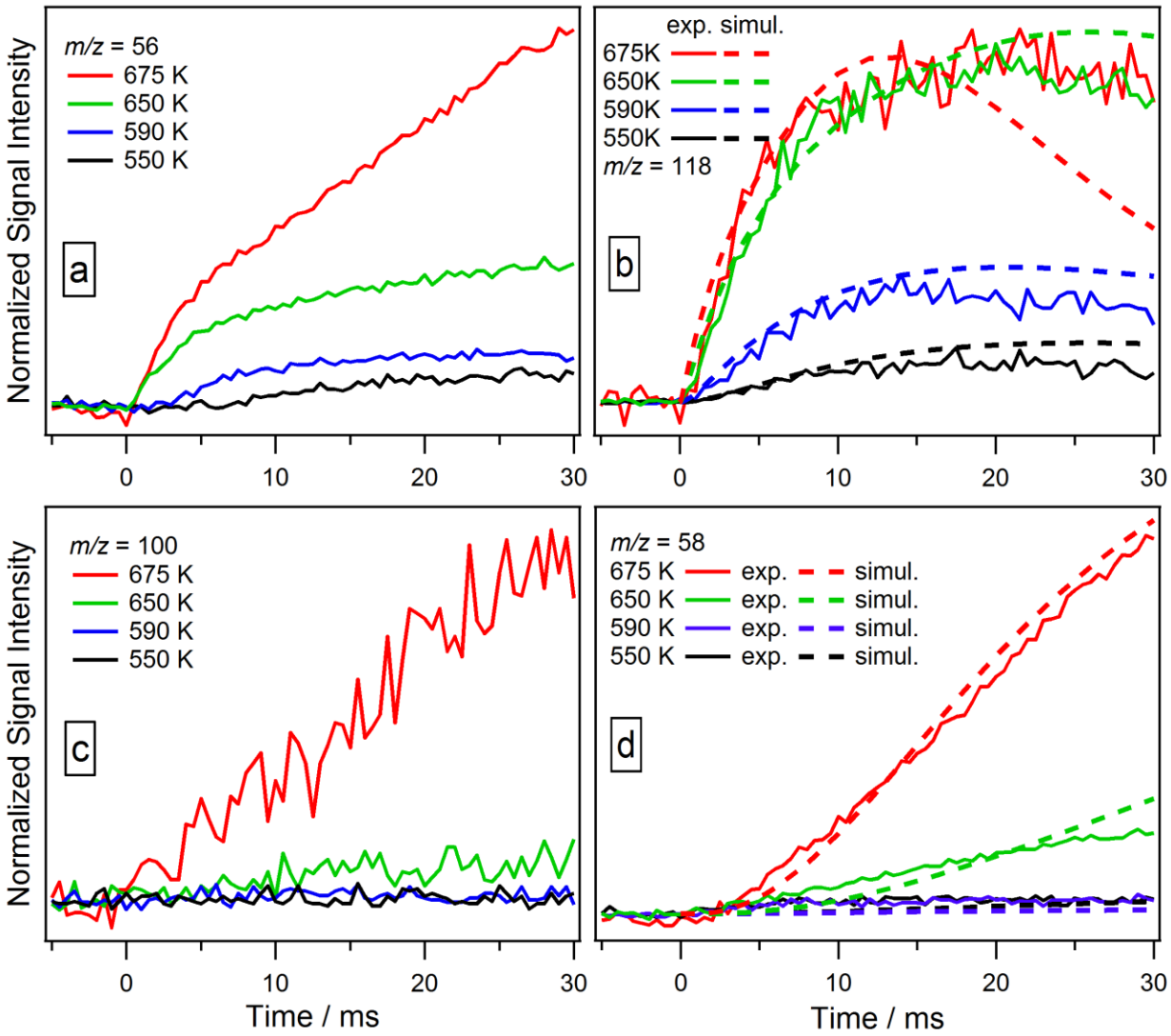

Figure 7. Comparison of time traces from a set of experiments using photolysis of highly stable $CFCl_3$ as Cl-atom source in neopentane oxidation experiments to reach higher temperatures without spontaneous oxidation of a reaction mixture. Note significant enhancement of oxidation upon increasing temperature from 650 to 675 K. Experiments were performed under constant density conditions ($[O_2] = 2.5 \times 10^{18}$ cm^{-3}) at about 1 atm pressure. A hydrogen discharge lamp was used for ionization. (**b,d**) Simulations were performed using NUIGMech_C5_July2015 model[14] with k'_{wall}(KHP) = 58 s^{-1} and are shown for comparison.

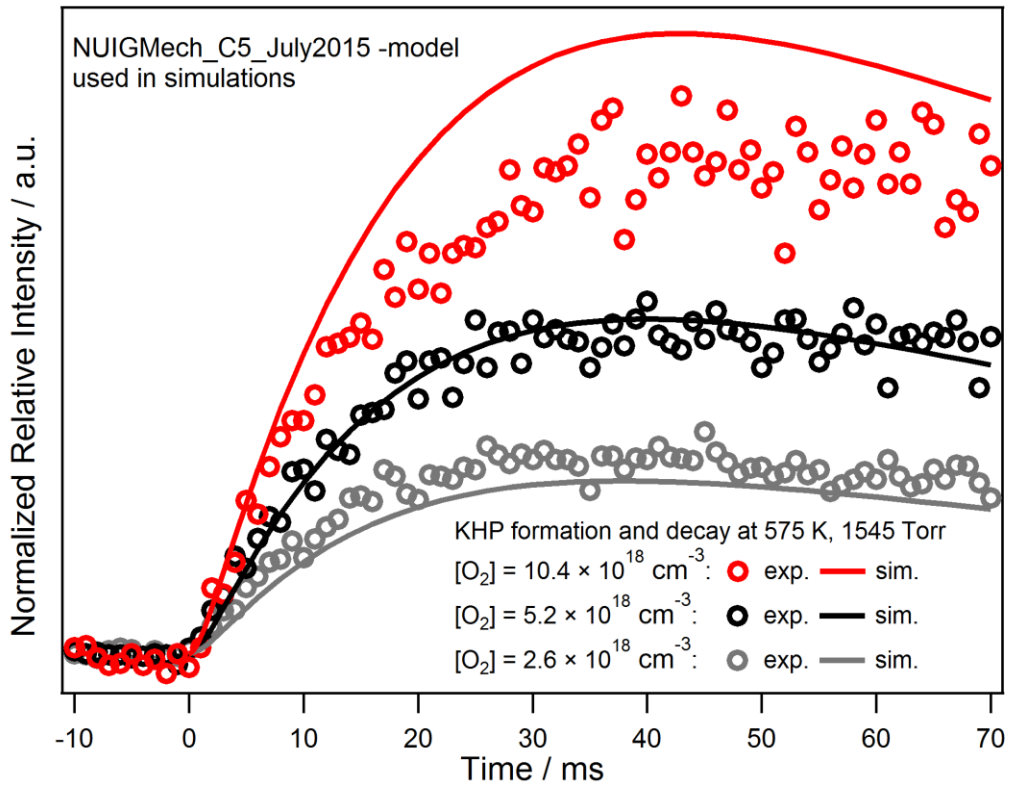

Figure 8. Experimental KHP formation and decay signals at 575 K, 1545 Torr pressure from a same set of neopentane oxidation experiments at three different oxygen concentrations. Signal intensities are normalized using oxygen signals. A hydrogen discharge (Lyman-α) radiation at 10.2 eV was used for ionization. Results of simulations using NUIGMech_C5_July2015 model[14] with k'_{wall}(KHP) = 29 s^{-1} are also shown for comparison.

Table 1. Experimentally determined branching ratios at 575 K/8.0 Torr, 625 K/8.7 Torr, and 675 K/9.4 Torr conditions (*i.e.* keeping total concentration constant) relative to *iso*-butene (*m/z* = 56). Branching ratios relative to species other than *iso*-butene can be obtained by dividing the corresponding values relative to *iso*-butene by each other. Stated uncertainties are based on statistical 1σ-uncertainties only. Employed [O_2] were 5×10^{16} cm^{-3}.

Product		Branching ratio relative to isobutene		
		575 K	625 K	675 K
3,3-Dimethyloxetane	(*m/z* = 86)	0.45 ± 0.05	1.21 ± 0.06	0.85 ± 0.04
2,2-Dimethylpropanal	(*m/z* = 86)	0.16 ± 0.02	0.12 ± 0.01	0.04 ± 0.02
2-Methyl-2-Propen-1-ol	(*m/z* = 72)	< 0.01	0.01 ± 0.01	0.02 ± 0.01
2,2-Dimethyloxirane	(*m/z* = 72)	< 0.02	0.02 ± 0.01	< 0.01
Methylpropanal	(*m/z* = 72)	0.04 ± 0.02	0.16 ± 0.02	0.08 ± 0.01
Propanal	(*m/z* = 58)	< 0.01	0.01 ± 0.01	< 0.01
Acetone	(*m/z* = 58)	0.04 ± 0.01	0.03 ± 0.01	0.02 ± 0.01
Formic acid	(*m/z* = 46)	-	0.05 ± 0.01	-
Acetaldehyde	(*m/z* = 44)	0.04 ± 0.01	< 0.02	< 0.01
Propene	(*m/z* = 42)	0.04 ± 0.01	< 0.02	0.02 ± 0.01
Formaldehyde	(*m/z* = 30)	1.25 ± 0.10	1.19 ± 0.05	0.60 ± 0.03
Ethene	(*m/z* = 28)	< 0.01	< 0.01	< 0.01

Table 2. Measured and simulated branching ratios (BRs) at 650 K, 1060 Torr determined relative to *iso*-butene (*m/z* = 56). Stated uncertainties are based on statistical 1σ-uncertainties only. Employed [O_2] was about 2.8 × 10^{18} cm^{-3}. Simulations were performed using NUIGMech_C5_July2015 model[14] with k'_{wall}(KHP) = 58 s^{-1}.

Product		BR(experimental) relative to *iso*-butene	BR(simulated) relative to *iso*-butene
3,3-Dimethyloxetane	(*m/z* = 86)	1.64 ± 0.33	2.50
2,2-Dimethylpropanal	(*m/z* = 86)	0.15 ± 0.02	-
2-Methyl-2-Propen-1-ol	(*m/z* = 72)	0.09 ± 0.05	0.03
2,2-Dimethyloxirane	(*m/z* = 72)	0.14 ± 0.08	0.06
Methylpropanal	(*m/z* = 72)	0.90 ± 0.18	0.03
Methacrolein	(*m/z* = 70)	< 0.04 ± 0.01	0.13
Propanal	(*m/z* = 58)	0.00 ± 0.03	< 0.01
Acetone	(*m/z* = 58)	0.75 ± 0.10	1.06
Formic acid	(*m/z* = 46)	0.40 ± 0.07	0.19
Acetaldehyde	(*m/z* = 44)	< 0.07	< 0.01
Propene	(*m/z* = 42)	0.39 ± 0.07	0.03
Formaldehyde	(*m/z* = 30)	3.00 ± 0.34	2.77
Ethene	(*m/z* = 28)	< 0.06	< 0.01
KHP	(*m/z* = 118)	-	2.36

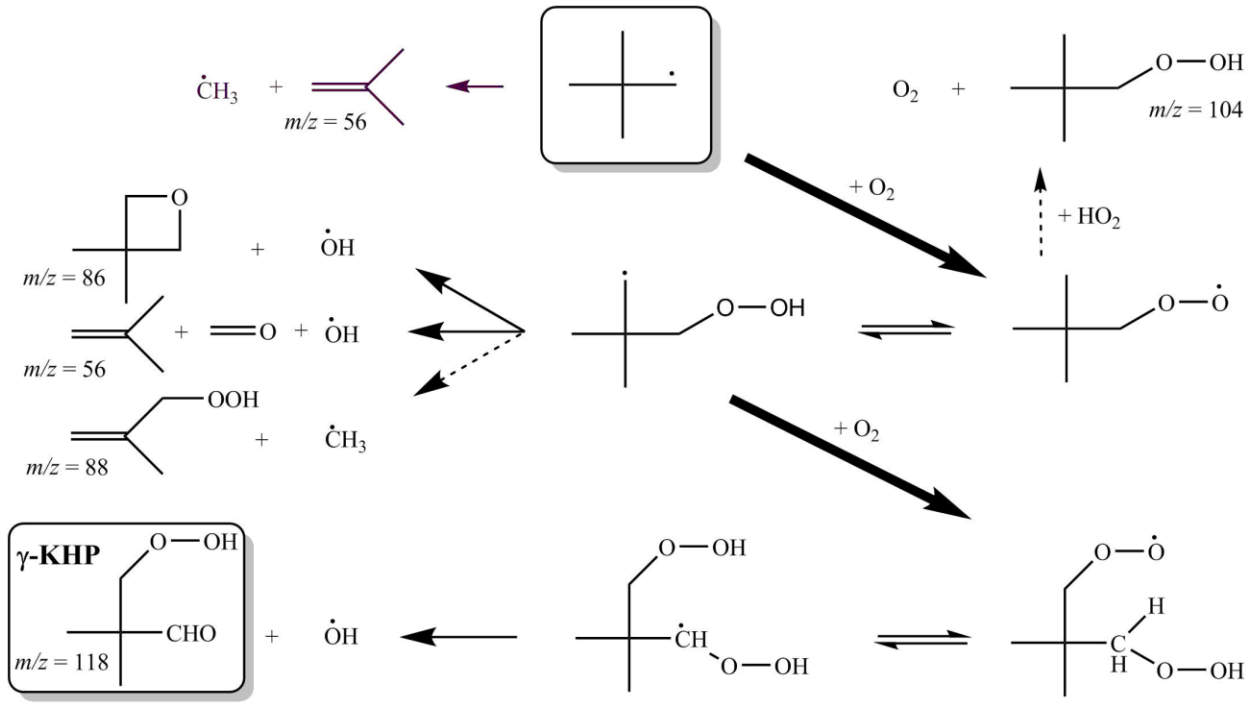

Scheme 1: Neopentane low-temperature oxidation reaction mechanism starting from neopentyl radical and extending up to γ-KHP formation.[10]

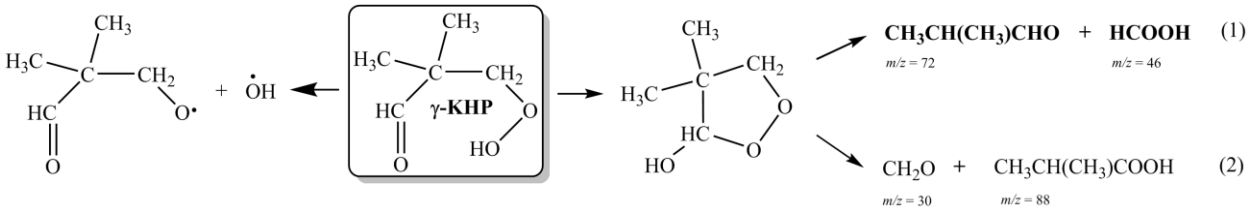

Scheme 2. γ-KHP decomposition *via* -O–OH bond rupture to two radicals (left) or through cyclic peroxide intermediate to carbonyl compound and organic acid (right), known as Korcek decomposition mechanism[27].

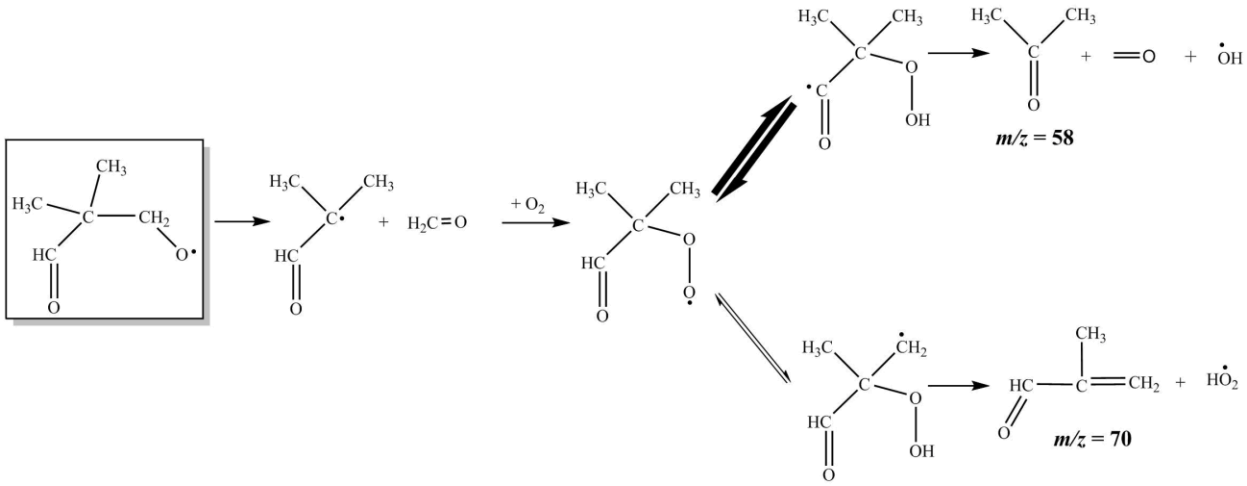

Scheme 3: Main pathways from isobutanal-2-methyloxy radical, formed in decomposition of γ-KHP to $HCOC(CH_3)_2CH_2O$ + OH, in neopentane low-temperature oxidation experiments.[10]

6. References

1. J. E. Dec, *Proc. Combust. Inst.*, 2009, **32** 2727-2742.
2. C. K. Westbrook, *Proc. Combust. Inst.*, 2000, **28**, 1563-1577.
3. H. Sun and J. W. Bozzelli, *J. Phys. Chem. A*, 2004, **108**, 1694-1711.
4. J. D. DeSain, S. J. Klippenstein and C. A. Taatjes, *Phys. Chem. Chem. Phys.*, 2003, **5**, 1584-1592.
5. R. R. Baker, R. R. Baldwin, C. J. Everett and R. W. Walker, *Combust. Flame*, 1975, **25**, 285-300.
6. R. R. Baker, R. R. Baldwin and R. W. Walker, *Combust. Flame*, 1976, **27**, 147-161.
7. R. R. Baker, R. R. Baldwin and R. W. Walker, *Combust. Flame*, 1970, **14**, 31-36.
8. R. R. Baldwin, M. W. M. Hisham and R. W. Walker, *J. Chem. Soc. Faraday Trans. 1*, 1982, **78**, 1615-1627.
9. H. J. Curran, W. J. Pitz, C. K. Westbrook, M. W. M. Hisham and R. W. Walker, *Proc. Combust. Inst.*, 1996, **26**, 641-649.
10. S. Wang, D. L. Miller, N. P. Cernansky, H. J. Curran, W. J. Pitz and C. K. Westbrook, *Combust. Flame*, 1999, **118**, 415-430.
11. P. Dagaut and M. Cathonnet, *Combust. Flame*, 1999, **118**, 191-203.
12. S. V. Petway, H. Ismail, W. H. Green, E. G. Estupiñán, L. E. Jusinski and C. A. Taatjes, *J. Phys. Chem. A*, 2007, **111**, 3891-3900.
13. J. Bugler, K. P. Somers, E. J. Silke and H. J. Curran, *J. Phys. Chem. A*, 2015, **119**, 7510-7527.
14. J. Bugler, B. Marks, O. Mathieu, R. Archuleta, A. Camou, C. Gregoire, K. A. Heufer, E. L. Petersen and H. J. Curran, *Combust. Flame*, 2016, **163**, 138-156.
15. F. Battin-Leclerc, O. Herbinet, P.-A. Glaude, R. Fournet, Z. Zhou, L. Deng, H. Guo, M. Xie and F. Qi, *Angew. Chem. Int. Ed.*, 2010, **49**, 3169-3172.
16. K. Moshammer, A. W. Jasper, D. M. Popolan-Vaida, A. Lucassen, P. Dievarti, H. Selim, A. J. Eskola, C. A. Taatjes, S. R. Leone, S. M. Sarathy, Y. G. Ju, P. Dagaut, K. Kohse-Hoinghaus and N. Hansen, *J. Phys. Chem. A*, 2015, **119**, 7361-7374.
17. A. J. Eskola, O. Welz, J. Zador, I. O. Antonov, L. Sheps, J. D. Savee, D. L. Osborn and C. A. Taatjes, *Proceedings of the Combustion Institute*, 2015, **35**, 291-298.
18. D. L. Osborn, P. Zou, H. Johnsen, C. C. Hayden, C. A. Taatjes, V. D. Knyazev, S. W. North, D. S. Peterka, M. Ahmed and S. R. Leone, *Rev. Sci. Instrum.*, 2008, **79**, 104103.
19. I. O. Antonov, J. Zador, B. Rotavera, E. Papajak, D. L. Osborn, C. A. Taatjes and L. Sheps, *J. Phys. Chem. A*, 2016, **120**, 6582-6595.
20. A. J. Eskola, O. Welz, J. D. Savee, D. L. Osborn and C. A. Taatjes, *J. Phys. Chem. A*, 2013, **117**, 12216-12235.
21. J. A. Montgomery, M. J. Frisch, J. W. Ochterski and G. A. Petersson, *J. Chem. Phys.*, 1999, **110**, 2822-2827.

22. M. J. Frisch, G. W. Trucks, H. B. Schlegel, G. E. Scuseria, M. A. Robb, J. R. Cheeseman, G. Scalmani, V. Barone, B. Mennucci, G. A. Petersson, H. Nakatsuji, M. Caricato, X. Li, H. P. Hratchian, A. F. Izmaylov, J. Bloino, G. Zheng, J. L. Sonnenberg, M. Hada, M. Ehara, K. Toyota, R. Fukuda, J. Hasegawa, M. Ishida, T. Nakajima, Y. Honda, O. Kitao, H. Nakai, T. Vreven, J. Montgomery, J. A., J. E. Peralta, F. Ogliaro, M. Bearpark, J. J. Heyd, E. Brothers, K. N. Kudin, V. N. Staroverov, R. Kobayashi, J. Normand, K. Raghavachari, A. Rendell, J. C. Burant, S. S. Iyengar, J. Tomasi, M. Cossi, N. Rega, N. J. Millam, M. Klene, J. E. Knox, J. B. Cross, V. Bakken, C. Adamo, J. Jaramillo, R. Gomperts, R. E. Stratmann, O. Yazyev, A. J. Austin, R. Cammi, C. Pomelli, J. W. Ochterski, R. L. Martin, K. Morokuma, V. G. Zakrzewski, G. A. Voth, P. Salvador, J. J. Dannenberg, S. Dapprich, A. D. Daniels, Ö. Farkas, J. B. Foresman, J. V. Ortiz, J. Cioslowski and D. J. Fox, *Journal*, 2009.
23. J.-D. Chai and M. Head-Gordon, *Physical Chemistry Chemical Physics*, 2008, **10**, 6615-6620.
24. I. R. Slagle, L. Batt, G. W. Gmurczyk, D. Gutman and W. Tsang, *J. Phys. Chem.*, 1991, **95**, 7732-7739.
25. A. Schweig, H. Vermeer and U. Weidner, *Chem. Phys. Lett.*, 1974, **26**, 229-233.
26. P. J. Linstrom and W. G. Mallard, eds., *NIST Chemistry WebBook, NIST Standard Reference Database Number 69*, National Institute of Standards and Technology, Gaithersburg, MD, 2012.
27. A. Jalan, I. M. Alecu, R. Meana-Paneda, J. Aguilera-Iparraguirre, K. R. Yang, S. S. Merchant, D. G. Truhlar and W. H. Green, *Journal of the American Chemical Society*, 2013, **135**, 11100-11114.
28. C. Bahrini, P. Morajkar, C. Schoemaecker, O. Frottier, O. Herbinet, P.-A. Glaude, F. Battin-Leclerc and C. Fittschen, *Physical chemistry chemical physics : PCCP*, 2013, **15**, 19686-19698.
29. A. Rodriguez, O. Herbinet, Z. Wang, F. Qi, C. Fittschen, P. R. Westmoreland and F. Battin-Leclerc, *Proceedings of the Combustion Institute*, DOI: http://dx.doi.org/10.1016/j.proci.2016.05.044.
30. M. Pelucchi, M. Bissoli, C. Cavallotti, A. Cuoci, T. Faravelli, A. Frassoldati, E. Ranzi and A. Stagni, *Energy & Fuels*, 2014, **28**, 7178-7193.
31. J. Bugler, A. Rodriguez, O. Herbinet, F. Battin-Leclerc, C. Togbé, G. Dayma, P. Dagaut and H. J. Curran, *Proceedings of the Combustion Institute*, DOI: http://dx.doi.org/10.1016/j.proci.2016.05.048.